JOURNAL OF MATERIALS SCIENCE 5 (1970) 53–62

# Beam-Induced Changes in the Scanning Electron Microscopy of Poly(oxymethylene)

J. W. HEAVENS, A. KELLER, J. M. POPE*, D. M. ROWELL†
*H. H. Wills Physics Laboratory, University of Bristol, Bristol, UK*

Samples of injection-moulded Delrin of a particular known morphology were examined in the scanning electron microscope. It was found that the beam affected the specimen in certain characteristic ways, the raster leaving a permanent imprint on the sample surface. By considering the nature of the irradiation process in the scanning electron microscope the amount and type of beam damage could be quantitatively correlated with the operating variables of the instrument. It is hoped that this will provide the groundwork for similar investigations on other systems. The importance of understanding and controlling beam-induced effects in the interpretation of scanning electron microscope images is clearly brought out by the present study.

The nature of the beam damage bears a relation to the texture of the sample as inferred by other means. Thus the scanning electron microscope can serve as a device for achieving controlled beam etching in service of structure studies.

## 1. Introduction

It has been known for some time that the conditions under which polymeric materials are examined in the transmission electron microscope influence the images observed. This has been demonstrated by the loss in diffracting power of polymer crystals examined under the electron beam [1-3]. In addition Andrews [4] observed further image changes long after the disappearance of diffracting conditions. Such latter changes have been reported again more recently and examined systematically by Dlugosz and Keller [5] in the course of both transmission and scanning electron microscopy. The latter instrument is rapidly gaining importance in the field of microtopography. It is therefore important to recognise changes induced in the specimen surface by the electron beam.

In this investigation the effects of electron beam irradiation in the scanning electron microscope (SEM) on bulk samples of "Delrin"‡ have been examined. This polymer has proved particularly susceptible to damage effects of an easily recognisable kind. It is used to illustrate the dependence of the nature and severity of the damage effects observed upon some irradiation parameters peculiar to the SEM.

## 2. Electron Irradiation in the SEM

The principles of the SEM have been fully reviewed elsewhere [6, 7]. However, we shall here briefly recapitulate those aspects of SEM operation which may affect radiation damage. In particular we shall discuss the influence of the variables in machine operation on the numbers and energies of electrons incident on the specimen surface. This includes the electron optical system and the scanning mode of irradiation.

The electron optical system produces an electron beam which, at the location of the specimen, can be characterised by its diameter, electron current density and energy distribution. If the beam is stationary it will penetrate a "drop" shaped region in the specimen having

*Now at Department of Physics, University of Sussex, Falmer, Brighton.
†Now at University of Zambia, Lusaka.
‡Delrin is a poly(oxymethylene) manufactured by Du Pont de Nemours and Co. Inc.

TABLE I Effects caused by changing the S E M controls

| | 1<br>Machine variable | 2<br>Main parameters affected | 3<br>Expected effects on irradiating conditions |
|---|---|---|---|
| 1 | Filament current<br>Grid bias<br>Final aperture size | $i$, $D$ | increase in $P$<br>small change in $D$ |
| 2 | Accelerating voltage | electron energies, | small change in $P$<br>increase in $D$ and $z$ |
| 3 | Lens current | $i$, $D$ | decreases $P$ and $D$ |
| 4 | Magnification control<br>(specimen height and orientation) | magnification factor, $M$<br>(hence $L_x$, $L_y$) | increases $P$<br>increases $\rho$ |
| 5 | Line time control | line time, $t$ | decreases $\rho$<br>increases $P$ |
| 6 | Frame time control | frame time, $s$ | increases $\rho$<br>decreases frequency of irradiation, $F$ |

All effects in column 3 correspond to an increase in the machine variable shown in column 1.

dimensions characteristic of the properties of both specimen and incident beam. Within this region the electron dose rate varies widely due to the energy and current density distributions in the beam. We will use an arbitrary parameter $i$ which represents the average number of electrons supplied to a volume of material with maximum radius $D$ and maximum depth $z$ in unit time. These three parameters will vary with the machine variables in the manner summarised in table I.

We will now consider the way in which the electron beam is scanned across the specimen surface. The beam is deflected in orthogonal $x$ and $y$ directions by potentials applied to deflector plates in the final lens. The resulting path followed by the beam, in normal operation, is shown in fig. 1. The $x$-deflection causes the beam to scan a line of length $L_x$ in a time $t$ (the line time). The displacement $W$ and the number of lines $n$ in one frame or raster are given by

$$W = \frac{tL_y}{s}; \tag{1}$$

$$n = \frac{s}{t}, \tag{2}$$

where $s$ is the time to scan one frame (the frame time). The machine controls allow us to vary $t$ and $s$ over a wide range.

The size and shape of the raster described on the specimen surface are determined by the maximum $x$- and $y$-potentials, the specimen/final

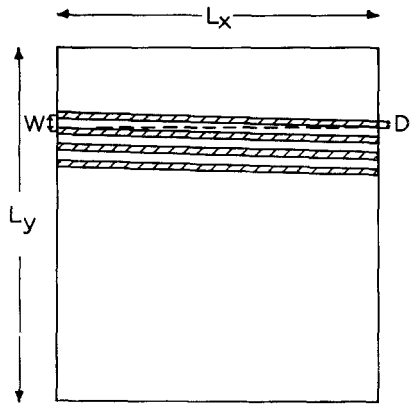


*Figure 1* Diagram of the path described on the specimen by the electron beam.

lens distance and the specimen orientation. These factors can be varied by means of the stepped magnification control and the specimen $z$ shift and tilt controls, respectively. The first two are used to determine a magnification parameter $M$ which is displayed on the machine.

For a specimen oriented normally to the incident beam the raster will be a square of side $L$ where

$$L = \frac{C}{M}; \tag{3}$$

$C$ is the display screen size and is a constant. In practice the specimen is deliberately tilted about the $x$-axis to improve electron collection and other tilts may arise if the specimen surface is not

parallel to the face of the mounting stub. Thus, in general, $L_x \neq L_y \neq L$. In the present work

$$L_x = L\,, \qquad (4)$$
$$L_y = \frac{L}{\cos 45°}\,.$$

Since the above correction applies to all the experiments we will ignore it in what follows.

From fig. 1 it can be seen that the specimen is irradiated in a number of parallel strips of width $D$, the effective spot diameter. The density of such strips $\rho$ (the line density) is given by:

$$\rho = \frac{n}{L} = \frac{Ms}{ct}\,. \qquad (5)$$

For complete irradiation in any one frame, without strip overlap, the parameters $t$, $s$, and $M$, must satisfy the relationship:

$$\frac{s}{t} = \frac{C}{DM}\,. \qquad (6)$$

If this equality does not hold then either non-irradiated or multiply-irradiated areas will occur. For a single line scan we can now define a "line dose density" $P$ where

$$P = \frac{ti}{L} = \frac{Mti}{C}\,. \qquad (7)$$

We note that this parameter defines the average number of electrons bombarding a unit length of line during one line scan. Assuming no overlap and exact superposition of lines in successive rasters we can also define a total line dose density $P_t$:

$$P_t = NP\,, \qquad (8)$$

where $N$ is the number of rasters scanned. The frequency $F$ at which $P$ is delivered to any line is determined by the frame time $s$ when the instrument is in normal operation.

From the above considerations we might expect that the severity of any beam damage effects would be related to $\rho$, $P$ and $F$, i.e.

$$\theta = \mathrm{f}(P, \rho, F)\,, \qquad (9)$$

where $\theta$ is any parameter which measures the severity of beam damage. In the experiments described below we attempt to ascertain the nature of this relationship by finding such a parameter $\theta$ and determining its dependence on the machine variables involved in the definitions of $P$, $\rho$ and $F$. The expected effects of a number of machine variables on these parameters are shown in table I.

## 3. Experimental

### 3.1. Material

The Delrin samples used were received in the form of injection moulded bars 5 in. × ½ in. × ⅛ in.* Previous investigations [8, 9] of the morphology of such samples revealed that the surface layers (originally in contact with the mould walls) consist of parallel lamellae oriented normally to the injection flow direction, hence also normally to the specimen surface. At a depth of 20 to 30 $\mu$m below the surface this structure gives way gradually to a more random spherulitic texture as shown in fig. 2.

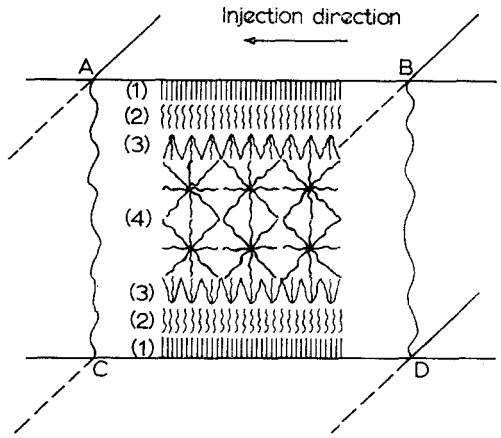


*Figure 2* Sketch illustrating diagrammatically the morphology of the injection moulded Delrin bars used in this work. The diagram is based on the polarising and transmission electron microscope studies of Clark [9] and Davis [8]. The plane ABCD is a cross-section parallel to the injection direction and perpendicular to the broad face of the "test piece" shaped object. The textures vary continuously from the surface towards the interior but can broadly be divided into four zones: (1) straight parallel lamellae (seen edge on); (2) twisting parallel lamellae; (3) sheaving lamellae; (4) spherulitic texture.

Specimens for examination in the SEM were mounted on aluminium stubs and coated with a thin (~ 500 Å) evaporated layer of 60/40% Au/Pd alloy to give the required electrical conductivity. Except where stated otherwise the results set out below were obtained on specimens with a surface, originally formed in contact with the mould walls, exposed to the electron beam.

*1 in. = 2.54 cm.

### 3.2. Irradiation Damage Effects

It was found that in all instances the beam profoundly affected the sample surface. This in itself means that the raster left a recognisable permanent imprint on the sample. Thus a square-shaped area scanned by the beam remained always distinctly different from the rest of the surface after examination. When with unaltered sample position the raster area was changed discontinuously (e.g. by changing magnification) then the areas which had been irradiated to different extents appeared as distinct concentric squares. Such a system of squares can be finally photographed under low powers, which produces only a minimum of beam damage in itself. In this way a permanent record of the effect of different irradiation conditions is obtained simultaneously on the same photograph. This procedure will be adopted throughout the present work.

A number of changes in surface morphology were observed during irradiation of specimens in the SEM. The most important ones are listed below:

(a) The scanned area is made visible, even after very short periods of irradiation in the form of a square shaped depression. This is first delineated by grooves along those two edges of the square which are parallel to the scanning lines (A in fig. 3).

(b) Cracks may form which appear to be oriented in a direction along which the surface lamellae are expected to lie (B in fig. 3). The edges of the cracks are usually bright, presumably due to anomalously low absorption of emitted electrons in these regions. The appearance of a well-defined crack is often preceded by a line of light contrast at the crack location. After further irradiation a fine structure of surface "wrinkles" appears between the cracks.

(c) A smoothing of the surface may occur causing the disappearance of prior surface detail (C in fig. 3). After further irradiation bubbles form which swell up and eventually burst leaving craters (D in fig. 3). Once surface-smoothing has occurred no further cracking takes place under *any* condition of irradiation. Hence this phenomenon is referred to below as stabilisation. Nevertheless on continued irradiation the smoothed out area becomes progressively further depressed – readily seen when the irradiated area is altered discontinuously (fig. 4). Combinations of these effects can be observed by changing the irradiation parameters as described below.

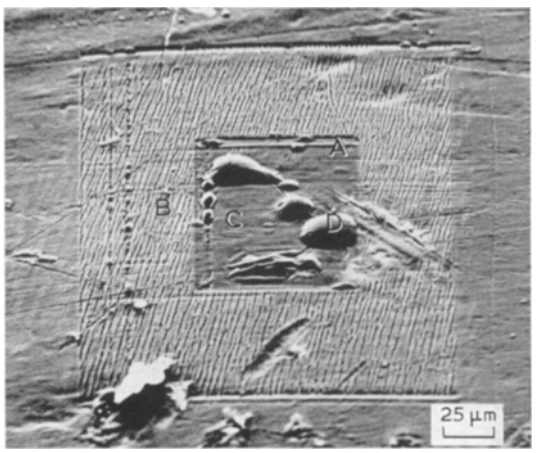


*Figure 3* Changes produced in a Delrin surface by irradiation in the SEM. Inner raster irradiated at a magnification of × 620 and outer at × 300. Faint cracks at far left are associated with a previous irradiation. For key to letters see text.

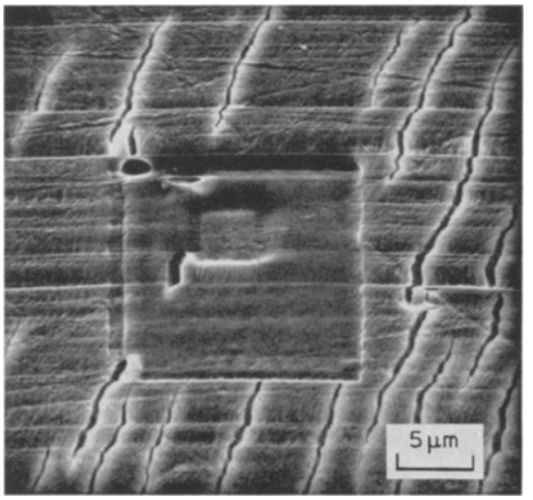


*Figure 4* "Stabilisation" of Delrin surface by irradiation at high magnification. Note fine structure between cracks and surface-smoothing and depression of stabilised region. Small innermost rasters and horizontal grooves in this and other micrographs are produced during focusing and contrast adjustment operations.

### 3.3. Effects of Changes in SEM Variables

In what follows, selected variables were systematically changed with the remainder held constant. Changes in surface morphology were observed and related to the number of rasters, $N^*$, needed to produce them. In general it was found that low values of the parameters $P$ and $\rho$ favoured crack-formation whilst high values led

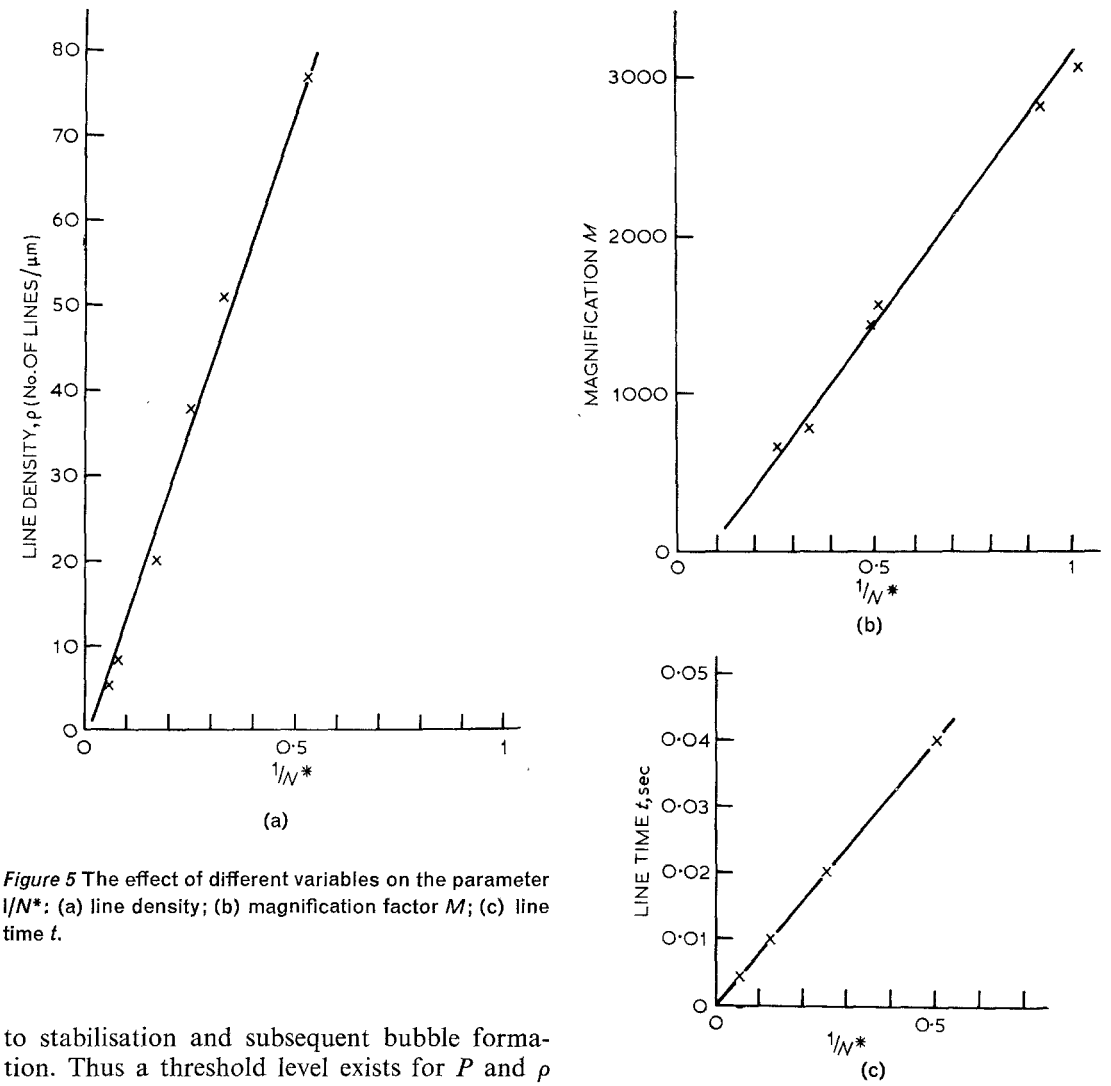


*Figure 5* The effect of different variables on the parameter $1/N^*$: (a) line density; (b) magnification factor $M$; (c) line time $t$.

to stabilisation and subsequent bubble formation. Thus a threshold level exists for $P$ and $\rho$ above which cracking will not occur. It was found that the stabilised conditions could be induced after one frame at the appropriate $P$- or $\rho$-levels without any visible change in the surface morphology occurring first. If the value of $P$ or $\rho$ was then reduced by, for instance, decreasing the magnification, cracking would only occur outside the original raster.

In the case of crack-formation it was found that the number of rasters required to produce cracking ($N^*$) was dependent on the machine variables defining the various irradiation parameters. Hence $1/N^*$ could be used as a measure of the severity of the irradiation damage effects resulting from one raster, and an attempt was made to determine the nature of the relationship in equation 9 with $1/N^*$ used as the parameter $\theta$. The experiments were carried out in the order suggested by consideration of table I and are described below.

The effects of changing the scanning frequency, $F$, were determined by introducing a delay between successive rasters. It was found that increasing the delay between rasters decreased $N^*$. For example, delays of 10, 65 and 125 sec gave $N^*$ values of 9, 7 and 6 respectively. Such changes only occurred for delay times much longer than those used during normal SEM operation. Hence frequency effects were assumed to be negligible during subsequent investigations.

The above assumption enabled the effects of changes in line density to be investigated by changing the frame time $s$. This is involved in the definition of $\rho$ but not in that of $P$. For a range of magnifications, $N^*$ was found to be inversely

proportional to the line density as shown in fig. 5a. A similar attempt was made to investigate the effect of the parameter $P$ through changes in the electron current density parameter $i$. However changes in $i$ proved difficult to monitor and the results were inconclusive. Better results in the study of the effect of $P$ were obtained by manipulating two of the three variables $s$, $t$ and $M$ to keep the line density $\rho$ constant while varying $P$. Thus by adjusting $M$ and $s$ with $t$ constant it was possible to show that $N^*$ is inversely proportional to $M$ (fig. 5b). If $M$ is kept constant and $t$ and $s$ manipulated a similar dependence of $N$ on $t$ is found to exist (fig. 5c).

Consideration of these results suggests that the form of equation 9 is

$$\frac{1}{N^*} \propto \rho P, \tag{10}$$

i.e. by substitution with equations 5 and 6

$$\frac{1}{N^*} \propto M^2 s \frac{i}{C^2}. \tag{11}$$

We note that the R.H.S. has the same units as the definition of dose used in more conventional irradiation techniques namely, number of electrons per unit area. This equation does not involve $t$ and experiment showed that $N^*$ was indeed independent of $t$ over the range 0.004 sec $< t <$ 0.4 sec, if all other parameters were kept constant.

In general, the variables discussed above did not affect the nature of the cracking produced if this was allowed to proceed to completion. However changes in accelerating voltage were found to have a profound effect on the lengths, spacings, and speed of propagation of the cracks (fig. 6a, b, c) although no marked variation in $N^*$ was observed. At 20 kV a crack, once initiated, rapidly extended over the whole length of the raster. As the accelerating voltage was reduced the cracks became shorter and more closely spaced. Below 5 kV the cracks that were formed rapidly widened and developed into small holes.

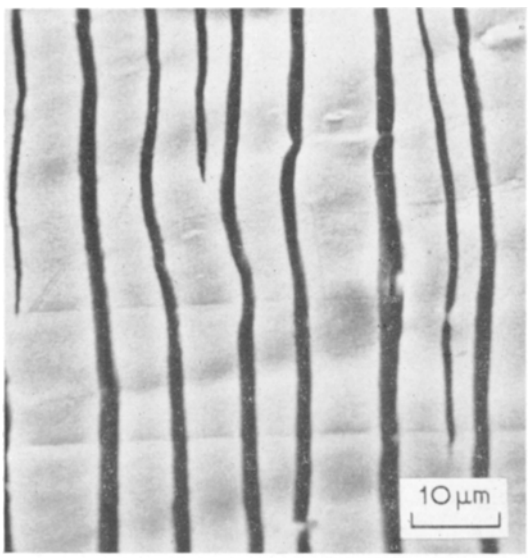


(a)

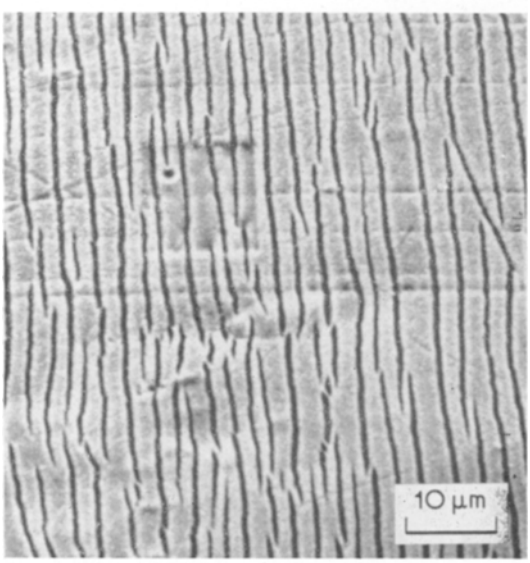


(b)

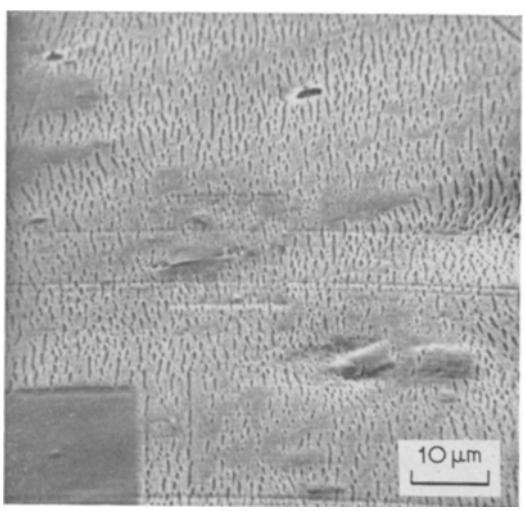


(c)

*Figure 6* The effect of changes in accelerating voltage on crack length and spacing: (a) 20 kV; (b) 10 kV; (c) 5 kV.

The effect of changing the thickness of the Au/Pd coating was also investigated. A specimen was first given a coating of normal thickness and then an electron microscope specimen grid used to mask parts of the surface whilst a second coating, ten times the thickness of the first, was applied. The grid was removed and the specimen examined in the SEM. Under conditions of low *P* both thinly and thickly coated areas were observed to crack but a greater density of cracks occurred in the former (fig. 7a). With increased *P*, surface-smoothing and bubble-formation occurred in the thickly coated region (fig. 7b) whilst the thinly coated areas continued to crack.

*Figure 7* Sample coated with two different thicknesses of gold palladium. Coating thickness in light areas is approximately ten times that in dark. (a) Irradiated at low *P*; (b) high *P*.

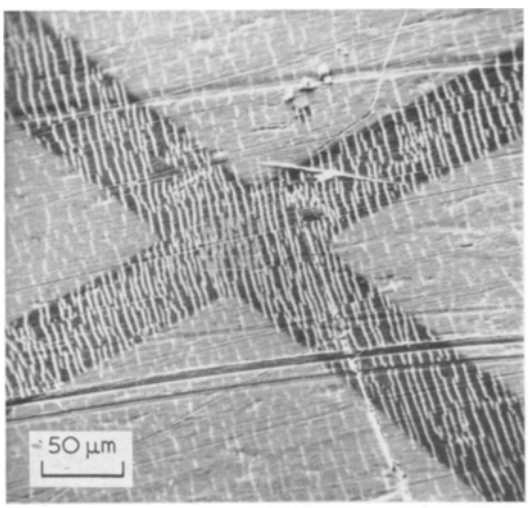


(a)

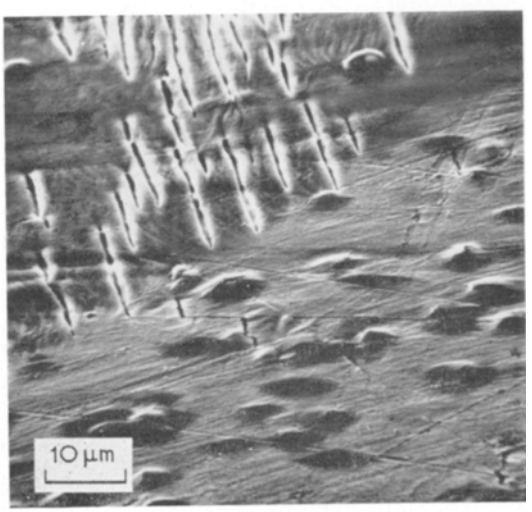


(b)

### 3.4. "Internal" Surfaces

Three techniques were used in trying to obtain surfaces representative of the interior structure of the bars. These were: (a) room temperature microtomy; (b) low temperature ultramicrotomy; (c) low temperature fracture. The microtome was used to remove slices from a Delrin block in order to expose the internal face shown in fig. 2. Surfaces exposed by method (a) were covered with knife marks and did not form cracks when irradiated although some smoothing and bubble-formation occurred. In this case the surface properties were probably radically altered by heating and plastic deformation. However, by using an ultramicrotome at liquid air temperatures deformation was considerably reduced and cracking was again observed. In the spherulitic part of the specimen the cracks were arranged in radial arrays whilst nearer the original specimen surfaces they became aligned. Both types of cracking are shown in figs. 8 and 9.

Similar results were obtained with low temperature fracture surfaces, although the surfaces were much rougher than for the ultramicrotome sections.

## 4. Discussion

### 4.1. On the Nature of the Beam Damage

Electron irradiation of materials in the SEM may produce two types of damage. First, local heating which may lead to physical or even chemical changes and also affect the surface morphology. Secondly, changes in chemical bonding due to direct interaction with the incident electrons. To date there are no data on these effects in the SEM, consequently we have to rely on information from other types of investigation, recognising that the metal coating with its differing electrical and thermal properties introduces additional problems.

Irradiation studies on Delrin using 1 MeV electrons revealed that both chain scission and cross-linking can occur [10]. The former is predominant, producing gaseous formaldehyde. The formation and bursting of surface bubbles in the present work suggest a similar, or at any rate gaseous, degradation product. Gas evolution was also observed by us when heating Delrin *in vacuo*,

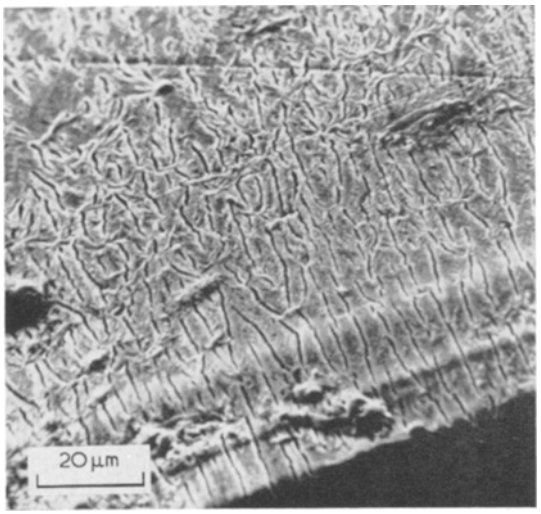


*Figure 8* Cracks in an internal surface of Delrin exposed by low-temperature ultramicrotomy. Note increasing randomisation of crack directions with distance from the surface of the material (cf. fig. 2).

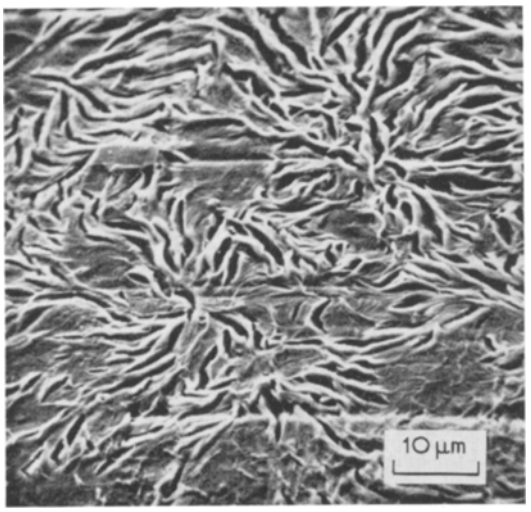


*Figure 9* Same specimen as fig. 8 but area irradiated is nearer to the spherulitic centre of the block (cf. fig. 2).

which indicates that this could also occur through the heating effect of the electrons in the SEM. The smoothing of the surface is certainly suggestive of melting; bubble-formation could then follow in the viscous molten medium. Heating effects, inferred in this way require a high initial electron dose, hence it appears that they occur only if the rate of energy deposition exceeds a critical value. Initial doses insufficient to produce smoothing lead to cracking. It is suggested that the stresses producing these cracks are generated by the formation of gas-filled subsurface voids. In the case of high doses when the surface is rendered plastic due to heat, these stresses would be relieved by homogeneous deformation such as bubble-formation. In the case of low doses with little heating these stresses can only be relieved by cracking. The lines of white contrast which precede cracking also suggests that subsurface voids form first.

The effect due to delays introduced between subsequent rasters is surprising. It implies that the degradation is continuing after the irradiation ceases.

The role of the thin Au/Pd coating layer requires separate attention. The metal layer will absorb a portion of the incident energy and hence shield the underlying substrate. Thus the decrease of cracking with increasing coating thickness is not unexpected. However, this does not explain the preferential formation of bubbles in thickly coated areas (fig. 7b). This may be due to higher temporary accumulation of heat at these highly absorbing localities. Little is known of how the surface coating accommodates changes in the surface morphology during irradiation. Nevertheless, there seems to be sufficient electrical continuity retained to prevent the "charging" effects normally observed with non-conducting materials.

The cracks produced by the radiation propagate parallel to the lamellar structure inferred from polarising microscopy (fig. 2) and thus appear to sever interlamellar ties. However, the intercrack spacing is much larger than the lamellar separation and in any case depends on irradiation conditions. The spacing decreases with the number of scanned rasters to a limiting value, which in itself decreases with decreasing electron energy, while the cracks become smaller. It is suggested that the cracks are initiated by flaws which may either be inherent in the lamellar texture or which had been introduced by the mechanical processing of the sample. In common with the general behaviour of brittle solids there should be a statistical distribution of such flaws, their number decreasing with increasing flaw severity. Cracks should form first at the most severe flaws within the area subjected to the tensile stress. Accordingly the spacings between cracks will be determined by the density of such flaws. Such considerations could account for the observed trend with changing voltage. Electrons of greater energy will penetrate deeper and this would lead to more extensive stress fields which, according to the foregoing, could

lead to increased intercrack spacings and also to longer cracks.

### 4.2. On the Significance of Line Dose Densities and Strip Densities

The more quantitative aspects of the work reveal the importance of both the line dose ($P$) and strip density ($\rho$). The dependence of beam damage on $\rho$ suggests either strip overlap in a single raster or the existence of some co-operation between separated strips to produce cracks. The condition for overlap is given by equation 6. This involves the effective strip width $D$. To evaluate $D$, $\rho$ was reduced so that individual strips of damage of measurable width became visible. Fig. 10 shows an example where an area was first irradiated with a raster containing only 20 lines and then photographed with a 1000 line raster. Here the visible strip width is 2 $\mu$m (compared with the 500 Å of the incident beam). This would give a strip overlap for $\rho > 5 \times 10^3$ lines/cm. Thus using equation 6 for a 1000 line raster, strip overlap would set in at a magnification of 500× and above. Since these are the conditions which apply throughout the work, strip overlap would occur giving rise to the density dependence in equation 10. However, the above method certainly overestimates the $D$ value pertaining under the usual conditions because it requires unusually long line times and hence large $P$. In fact when $P$ was lowered a reduction in $D$ was indeed observed. Accordingly, the above deduction of strip overlap may be questionable. On the other hand cracks can extend across adjacent though discrete lines of damage (fig. 11), which suggests that co-operative effects between separate lines may also cause or contribute to the line density effect in question.

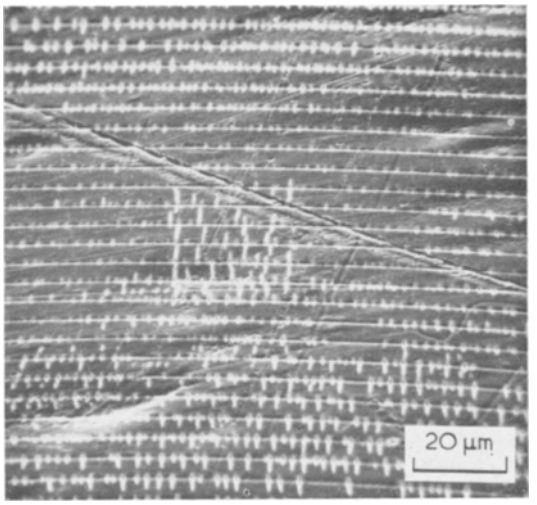


*Figure 10* Raster irradiated with $t = 1$ sec and $s = 20$ sec to reveal individual lines of damage (line width 2 $\mu$m approx).

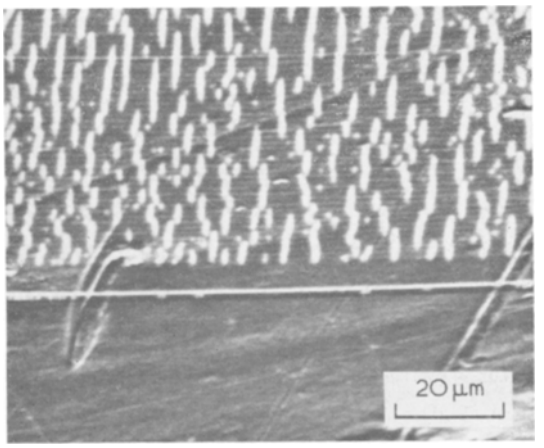


*Figure 11* Part of raster irradiated with $t = 0.2$ sec and $s = 20$ sec. Individual lines of damage are still visible (as fine horizontal striations) but cracks extend across many such lines.

### 4.3. General Implications for the Electron Microscopy of Polymers

Irrespective of why it occurs the principal conclusion that the electron beam changes the surface morphology of Delrin remains valid. As can be seen the nature of these changes is influenced by machine variables that are frequently changed during the course of a normal SEM investigation. Such phenomena need to be recognised so that the structures produced are not attributed to the original polymer surface without further qualification. Although Delrin may represent an extreme case, beam damage effects have also been observed in polyethylene [5] and similar changes could occur also in other polymeric materials.

The consequence of these changes need not be entirely negative, but could be put to use in the study of the true surface texture. The crack patterns produced clearly reflect both lamellar and spherulitic textures such as are expected to be present in the particular orientations actually observed. Hence the beam appears to bring out structures which we know ought to be there. Nevertheless, considering, say, the lamellar structure, we see that the crack-spacing varies with operating conditions, and therefore to have confidence in a one-to-one relation between

beam-induced image and intrinsic structure the appropriate irradiation conditions need to be assessed. Since in the SEM we have no complete freedom to choose our conditions for viewing at a particular resolution and as the image may change during viewing in any case, the utilisation of beam effects for the study of surface structure would require replication of the appropriately irradiated area for subsequent examination with the conventional transmission electron microscope.

In fact "etching" with ionising radiation coupled with replication is a well known technique for the study of polymer surfaces in transmission electron microscopy. However, there is no unanimous agreement as regards the reliability of the information obtained in this way [11, 12]. We see from the present work that doubts about the uniqueness of beam-induced surface structures are justified. The SEM however, could serve to define conveniently the optimum conditions of beam etching in a controlled way, to be utilised in studies with the transmission electron microscope.

Naturally in order to retain the principal advantages of the SEM, i.e. no need for elaborate specimen preparation methods and large depth of focus, one would like to use it without recourse to transmission electron microscopy. In the light of the present work it will be apparent that in doing so the possible beam-induced changes, whether beneficial or harmful for the purpose in question, will need individual assessment in every case. As far as reduction of beam-induced effects is desirable it is hoped that the present study has laid out some of the factors which need to be appreciated for this purpose.

## Acknowledgement

We are indebted to Professor H. E. Hinton for provision of SEM facilities, and to Dr E. S. Clark of du Pont de Nemours Inc, Wilmington, USA for providing the samples together with the relevant information. Two of us (J.W.H. and J.M.P.) would like to thank the Science Research Council for financial support.

## References

1. A. KELLER and D. C. BASSETT, *Proc. Roy. Microscop. Soc.* **79** (1960) 243.
2. A. KELLER (appendix with R. ENGLMAN) *J. Polymer Sci.* **36** (1959) 361.
3. P. GEIL, "Polymer Single Crystals" (Interscience, Wiley, 1963).
4. E. H. ANDREWS, *Proc. Roy. Soc.* **A270** (1962) 232.
5. J. DLUGOSZ and A. KELLER, *J. Appl. Phys.* **39** (1968) 5776.
6. C. W. OATLEY, W. C. NIXON, and R. F. W. PEASE, *Adv. Electr. Electr. Phys.* **21** (1965) 181.
7. P. R. THORNTON, "Scanning Electron Microscopy" (Chapman and Hall, London, 1968).
8. H. A. DAVIS, *J. Polymer Sci.* A2 **4** (1967) 1010.
9. E. S. CLARK, *S.P.E. Jnl.* **23** (1967) 46.
10. H. VON FISCHER and W. LANGBEIN, *Kolloid Z.u.Z. Polymere* **216-217** (1967) 329.
11. M. KUROKAWA, N. MOTOJI, and T. BAN, *J. Electr. Micros.* **13** (1964) 195.
12. E. W. FISCHER, H. GODDAR, and G. F. SCHMIDT, *Kolloid Z.u.Z. Polymere* **226** (1968) 30.

Received 25 June and accepted 20 September 1969.